Time-coded neurotransmitter release at excitatory and inhibitory synapses

Serafim Rodrigues[i] [*], Mathieu Desroches[i] [†], Martin Krupa[i] [†], Jesus M Cortes [‡] [§] [¶], Terrence J. Sejnowski [‖] [**] [††] and Afia B Ali[i] [‡‡]

[*]School of Computing and Mathematics, University of Plymouth, UK,[†]Inria Paris-Rocquencourt Research Centre, Le Chesnay, France,[‡]Biocruces Health Research Institute, Cruces University Hospital, Plaza de Cruces S/N, 48903, Barakaldo, Bizkaia, Spain,[§]Ikerbasque, The Basque Foundation for Science, Alameda Urquijo, 36-5 Plaza Bizkaia, 48011 Bilbao, Bizkaia, Spain,[¶]Departamento de Biologia Celular e Histologia, University of the Basque Country, Barrio Sarriena s/n, 48940 Leioa, Bizkaia, Spain,[‖]The Computational Neurobiology Laboratory,[**]Howard Hughes Medical Institute, Salk Institute, La Jolla, CA 92037, USA,[††]Division of Biological Science, University of California, San Diego, La Jolla, CA 92093, USA, and [‡‡]UCL School of Pharmacy, Department of Pharmacology, University College London, UK.

Submitted to Proceedings of the National Academy of Sciences of the United States of America

Communication between neurons at chemical synapses is regulated by hundreds of different proteins that control the release of neurotransmitter that is packaged in vesicles, transported to an active zone, and released when an input spike occurs. Neurotransmitter can also be released asynchronously, that is, after a delay following the spike, or spontaneously in the absence of a stimulus. The mechanisms underlying asynchronous and spontaneous neurotransmitter release remain elusive. Here we describe a model of the exocytotic cycle of vesicles at excitatory and inhibitory synapses that accounts for all modes of vesicle release as well as short-term synaptic plasticity (STSP). For asynchronous release the model predicts a delayed-inertial protein unbinding associated with the SNARE complex assembly immediately after vesicle priming. New experiments are proposed to test the model's molecular predictions for differential exocytosis. The simplicity of the model will also facilitate large-scale simulations of neural circuits.

Neurotransmitter release, exocytotic-endocytotic cycle, SNARE and SM protein complexes, Short-Term Synaptic Plasticity | Activity-induced Transcritical Canard | SCA interneurons | CA1 hippocampus | Delayed-Inertial protein unbinding

Abbreviations: STSP, Short-Term Synaptic Plasticity; MT, Markram-Tsodyks model

Classification: Neuroscience, Physics

Corresponding Author

Terrence J. Sejnowski,
The Computational Neurobiology Laboratory and
Howard Hughes Medical Institute, Salk Institute,
La Jolla, CA 92037, USA
Division of Biological Science
University of California, San Diego, La Jolla, CA 92093, USA
email: sejnowski@salk.edu

Significance Statement Neurotransmitter exocytosis and STSP regulate large-scale brain electrical activity. This is the first study proposing a multi-timescale model, which is parsimonious yet with enough descriptive power to express on one hand the interactions between the SNARE and SM-protein complexes mediating all forms of neurotransmitter release and STSP, and on the other, electrical activity required for neuronal communication (i.e. it bridges between the microscopic and the mesoscopic). A key finding is the discovery of a mathematical structure termed, *activity induced-transcritical canard*, which quantifies and explains delayed and irregular exocytosis. This structure also paves a novel way to understand delayed and irregular processes (i.e. linked to sensitivity to initial conditions) across various biology processes.

Introduction

Molecular and electrophysiological data have revealed differences in the regulation of presynaptic exocytotic machinery giving rise to multiple forms of neurotransmitter release: Synchronous release promptly after stimulation, delayed asynchronous release and spontaneous release. Synchronous release is induced by rapid calcium influx and, subsequently, calcium-mediated membrane fusion [1]. Asynchronous release occurs only under certain conditions [1, 2]. Finally, spontaneous "mini" releases occur in the absence of action potentials [2].

Two distinct mechanisms have been proposed to explain the various modes of exocytosis. One view suggests distinct signalling pathways and possibly independent vesicle pools [3, 4]. The second and more parsimonious view argues that the three modes of release share key mechanisms for exocytosis, specifically, the canonical fusion machinery that operates by the interaction between the SNARE (soluble N-ethylmaleimide-sensitive factor, NSF, attachment protein receptor) proteins and SM-proteins (Sec1/Munc18) [5, 6, 7, 8, 9, 10]; see Fig.1. The SNARE proteins: syntaxin, SNAP-25 (25 kDa synaptosome-associated protein) and VAMP2 (vesicle-associated membrane protein, also called synaptobrevin 2), localized on the plasma membrane and the synaptic vesicle, bind to form a tight protein-complex, bridging the membranes to fuse.

The canonical building block forms a substrate from which the three release modes differentially specialise with additional regulatory mechanisms and specific $Ca2^{+}$ sources(s) and sensor(s) that trigger the exocytosis cycle. Calcium sensors for synchronous release have been identified as synaptotagmin (e.g. Syt1, -2 and -9). In contrast, for asynchronous and spontaneous release it remains unclear and controversial. However, experiments suggest multiple mechanistically distinct forms of asynchronous release operating at any given synapse and these have been associated for example with VAMP4, synaptotagmin (Syt7), Doc2 (still controversial), RIM proteins, phosphoprotein isoforms synapsin (Syn I and Syn II),

[i]Authors with equal contribution

Reserved for Publication Footnotes

endocannabinoids [11, 12, 13, 14, 15, 16]. These views are still being debated due to fragmentary and conflicting data (see review [17]). In addition, synaptic molecular machinery also regulates STSP, however, it is unclear how the molecular mechanisms underlying STSP and exocytotic-endocytotic release are integrated [18].

The present study proposes a semi-phenomenological multi-timescale model to explain the three modes of release as well as STSP in a unified framework. The model is derived via mass-action laws (see Supplementary Information - SI) and is based on the biological parsimonious model viewpoint pioneered, in particular, by Thomas Südhof [19] (see also SI for a summary). The resulting mathematical model describes the canonical SNARE and SM-protein interaction exocytotic cycle at a mesoscopic scale and therefore bridges the gap between molecular protein interactions and electrical synaptic activity, as observed in synaptic dual whole-cell recordings.

SNARE-SM Model assembly

To circumvent the prohibitive complexity of modeling, all proteins and detailed (as well as unknown) protein interactions involved in the exocytotic process, we propose to model the interaction of protein complexes semi-phenomenologically. That is, a mesoscopic viewpoint is assumed and first principles of mass-action laws are employed. In addition, in attempt to reduce the complexity of the physiological process, principles of nonlinear dynamics and multi-timescale dynamical systems theory are invoked [20, 21, 22, 23]. This results in a deterministic two-dimensional model, with variables (p_1, p_2), describing the interactions between the canonical SNARE and SM-protein complexes; hence the name SNARE-SM model (see SI). The remaining known exocytotic proteins are considered as regulatory processes and therefore are treated as parameters that can be tuned to obtain the different modes of release, as idealised in Fig.2.

There are numerous regulatory proteins, however only certain proteins are expressed at any given type of synapse (e.g., in Fig.2, VAMP4 and Syt 7 may not be expressed simultaneously). This suggests lumping certain proteins into a single mesoscopic parameter. In contrast, proteins that are shared between different release modes (e.g. Syt1, Syt2, Complexin, RIMs, Doc2, TRPV1 and VDCC) remain ungrouped. This results in a minimal set of nine parameters that are associated to the regulatory proteins (see model derivation in SI for further biophysical interpretation of the model's parameters).

An important regulatory parameter is the positive small parameter $0 < \varepsilon \ll 1$, which induces a separation of timescales between p_1 and p_2. Specifically, p_1 corresponds to a slow acting protein complex while p_2 is a fast acting protein complex. The remaining parameters regulate the interaction strength between p_1 and p_2 as well as the conformational changes of the individual protein complexes. The resulting model expresses features of slow, evoked irregular and spontaneous activation. These features emerge from the rules of interaction between the protein complexes (p_1, p_2) as expressed by the right-hand side of the SNARE-SM model equations (SI). These interactions are best described (in mathematical terms) by plotting the components of the rules (technically, *nullclines*) in a two-dimensional space (*phase-space*) spanned by the actions of p_1 and p_2 (see Fig.3-a and Fig.S1-c). In particular, the interaction between p_1 and p_2 give rise to special configuration points, namely S (*stable equilibrium*), U (*unstable equilibrium of saddle type*), SN (*saddle-node* point) and TC (*transcritical* point) (see Fig.3-a and Fig.S1-c), which generate all the functions associated with each stage of the exocytosis-endocytosis cycle. In particular, S can be associated to Munc13-1 forming a homodimer that inhibits priming. Then, U can be related to the action of Munc13 gating the transition from closed-Syntaxin/Munc18 complex to the SNARE complex formation. Subsequently, TC can be linked to the action of complexin and finally, SN can be connected to the refilling of the vesicle pool. It is noteworthy to observe that the resulting phase-space geometry of the mathematical model shares a great deal of similarity with the schematic diagram of the SNARE-SM biological model by T. Südhof; compare Fig-3-a and Fig.S1-c with Fig.S1-a. Moreover, the model variables can be activated by a presynaptic stimulus (e.g. calcium influx), represented by the variable $V_{in}(t)$. By means of control parameters the three modes of neurotransmitter release are mathematically translated into the model's dynamic repertoire: *excitability*, *delayed response to input stimuli* or *limit-cycle dynamics* (SI). Importantly, the SNARE-SM model is sensitive to initial conditions without generating chaos. This sensitivity constitutes the core mechanism that governs the irregular activation. Moreover, due to the timescale separation between p_1 and p_2, the delayed neurotransmitter release results from the protein-protein binding and subsequent unbinding that occurs with inertia.

The delay is specifically explained by a novel mathematical structure that acts as a dynamic (delayed) response to an input via transcritical canards [22, 23], which we denote, *activity-induced transcritical canards* (SI). This structure quantifies the delay and predicts a delayed-inertial protein unbinding associated with the SNARE complex assembly immediately after vesicle priming. This novel approach is in stark contrast to previous modeling attempts that employ stochastic elements or hardwire a delay into the model to account for asynchronous release [24, 25, 26, 27, 28]. In contrast, the delay in the SNARE-SM model emerges as a result of a dynamic mechanism that is suggestive of a biological process.

In brief, the SNARE-SM model has a mechanistic interpretation since it can be related to processes associated with exocytotic-endocytotic signalling pathways, including intracellular calcium dynamics. Moreover, the delayed irregular activation can be associated, e.g., with the action of complexin, Syn I (II), the presence of endocannabinoid, VAMP4, or even Doc2 in the case of excitatory neurons.

Extended SNARE-SM model: E-SNARE-SM. We extend the SNARE-SM model to show how STSP mechanistically integrates within the exocytotic-endocytotic machinery, and also to enable comparison with electrophysiological data. This is achieved by feeding the exocytotic-endocytotic signal of the SNARE-SM model into an STSP model, which effectively activates the vesicle pool. In particular, we use the Markram-Tsodyks (MT) STSP model [29, 30, 31](SI). The MT equations phenomenologically model the time evolution of available resources (vesicles) and how efficiently neurotransmitters are released. This is represented by two quantities, namely, the amount of vesicles, d, and the release probability, f, which are updated for every pre-synaptic spike occurring at time instant t_s. This in-turn quantifies the amount of neurotransmitter released, $T(t_s) = d(t_s)f(t_s)$, which in reality is released with a small time delay.

The MT-model successfully accounts for the highly heterogeneous STSP dynamics across different brain areas in the context of synchronous release (see Table S1 in [31]). Consequently, the proposed model extends the MT-model by incorporating all three modes of neurotransmitter release observed at unitary synapses. However, to complete the model framework and to enable testing against data sampled from whole-cell paired-recordings obtained from unitary synapses, an ob-

servational variable representing post-synaptic potentials is required. This is modeled with the standard conductance-based (sub-threshold) equation, where the action of neurotransmitters on post-synaptic neurotransmitter receptors follows first-order kinetic equation (SI). More detailed approaches for modeling receptor dynamics (e.g. detailed kinetics [32]) will be a matter of future considerations.

Results

SNARE-SM Model dynamics: The SNARE-SM model has three operating modes. Fig.3-a shows a presynaptic terminal, which encloses the SNARE-SM model's signalling mechanism. The black arrows labeled p_1 and p_2 span the two-dimensional space within which the protein complexes interact. This is not a physical space, but rather a phase space where protein functions take place and the values of p_1 and p_2 represent the levels of activity between protein complexes. The line Γ_1 and the parabola Γ_2, called the fast nullclines, indicate the regions in which the functions of the protein complexes are quasi-stationary (Fig.3-a and Fig.S1-c). The line Γ_1 is stable to the left of the transition point TC; the parabola Γ_2 is stable above the transition point SN. Past the transition points, the fast nullclines become unstable (dashed lines). For clarity, the slow nullclines are not displayed (SI).

The stability of the fast nullclines is assessed by looking at the mathematical limit of the model when p_1 is kept constant ($\varepsilon = 0$); see SI for details. In this limit, the only variable left is p_2, and p_1 acts as a parameter; the equilibrium states lie on the fast nullclines and their stability depend on the parameter p_1 and change at bifurcation points SN and TC. Under normal operating conditions ($\varepsilon > 0$), p_1 evolves slowly; the points SN and TC are not anymore bifurcation points of the model; however, they still organise dynamic transitions between different levels of quasi-stationary activity close to Γ_1 and Γ_2. Moreover, the SNARE-SM model possesses two true stationary states, marked S and U (Fig.3-a and Fig.S1-c), which endow it with an excitable structure.

An exocytotic signal (red trajectory) is evoked by one or more presynaptic spikes. Input stimuli excite the system away from the functionally-inactive state S. However, the protein complexes switch their functional behaviour past the switching point (U) only when sufficient energy is available, via action potentials and increase in calcium influx. In this case, the system passes the TC transition point, which enables the appropriate exocytotic signalling mode to be activated. Fig.3-b illustrates the process in the time domain: Fig.3-b1 shows the presynaptic stimulus; Fig.3-b2 shows the output signal; Fig.3-b3 is a schematic diagram that depicts a particle, initially at a rest point (S), that is driven out of the basin of attraction of S by a sufficient force (blue arrows) enabling it to jump the energy barrier (U) [33]. This is an example of an excitable state, in which a particular amplitude and timing of a perturbation can drive the system away from the equilibrium point and induce it to make a large-amplitude, transient excursion before it settles again to its inactive state (S).

Past the switching point (U), the protein complexes p_1 and p_2 begin to interact strongly, activating states associated to vesicle priming I. The passage through the TC point can be associated with the initiation of priming stage II (i.e. SNARE-complex assembly and regulation by complexin). Priming can be a fast (synchronous) or a slow (asynchronous) process, depending on the timescale parameter ε.

From a mathematical perspective, precise quantitative control of the delay is achieved by the so-called "way-in-way-out function" (SI). In short, the activity-induced transcritical canard predicts the existence of delayed-inertial protein unbinding occurring between priming I and fusion-pore opening stages. This can be possibly related to the clamping action of complexin, or Ca^{2+}-activated calcium sensors (e.g. Synaptotagimin-1) competing with complexin for SNARE complex binding (by displacing part of complexin within the SNARE but via a delayed inertial unbinding). Indeed from the modelling point of view, ε (which also controls the delayed process), can at a molecular level be associated with complexin or (a)synchronous calcium sensors (see SI). The unbinding between p_1 and p_2 (e.g. interpreted mesoscopically as translocation of complexin) initiates fusion (F) and subsequent neurotransmitter release. Following exocytosis, p_1 and p_2 begin a second phase of strong interaction that induces endocytosis (E) and subsequent vesicle refilling (R). The final stage is triggered by the SN transition point, which prompts p_1 and p_2 to alter their states and evolve towards their inactive state S, where the vesicle pool is replenished.

SNARE-SM model evoked release mode. Evoked synchronous and asynchronous modes of release in the SNARE-SM model are shown in Figs. S2-S6 with the parameters in Table S1. For the synchronous mode, Fig S3 shows that the SNARE-SM model's output, p_2, is activated almost instantaneously upon an incoming stimulus, V_{in}. In this case, ε has a small value. Increasing ε induces a weaker binding/unbinding that effectively introduces variability (irregular activation via sensitivity to initial conditions) and a strong inertia in the unbinding process, causing a delay. This asynchronous mode is shown in Fig.S4, where the onset of p_2 is delayed with respect to the stimulus. Note that the output time profile also changes shape and amplitude, with a slower rising phase. These are crucial features that lead to gradual activation of vesicle pools as well as postsynaptic receptors, consistent with the gradual postsynaptic potential response observed in experiments for asynchronous release [1].

Fig.S2 shows three different delayed responses under the same two-spike stimulus, demonstrating irregular activation due to the model's sensitivity to initial conditions. Moreover, a burst of spikes may be required before the vesicle pool is activated, a feature that is widely reported in experiments [1]; this is controlled by increasing the distance between the two configuration states S and U, thereby increasing the energy barrier (Fig.3-b3). The farther they are apart, the stronger the stimulus (multiple spikes) that is needed to elicit vesicle priming (P). A delayed response to a stimulus with three spikes is shown in Fig.S5. Note that if the interspike interval between input stimuli is smaller than the exocytotic-endocytotic cycle time, then the delay decreases inversely to the input frequency increase. However, this delay does not decrease below a fixed value that corresponds to synchronous release.

SNARE-SM model spontaneous release mode. There are two different ways to generate spontaneous "mini" releases in the SNARE-SM-model as illustrated in Fig.S6 panels a1-b1 and a2-b2, respectively. One way is to assume that Ca^{2+}-channels open stochastically, which changes the resting baseline of Ca^{2+}-concentrations [2]. This is accomplished by decreasing the amplitude of the parabola Γ_2, which changes the fusion dynamics. This change can be related to empirical data showing the existence of multiple-fusion processes, such as kiss-and-run, clatherin-dependent endocytosis and bulk endocytosis [34]. Kiss-and-run is relevant to spontaneous release, where vesicles do not fuse entirely with the membrane and thus are rapidly retrieved from the active zone (release site).

The model also needs to be in a strongly excitable regime, in which the two configuration states S and U are sufficiently close to each other. As a consequence, low-noise perturba-

tions are sufficient to kick the system away from its inactive state (S) to complete endocytosis before settling back to S (Fig.S6-b2). An alternative mode of spontaneous release is via Ca^{2+}-sparks from internal Ca^{2+}-stores [1, 2]. This stimulates a limit cycle (a self-sustained periodic signal) (Fig.S6-b1) that is achieved by moving both the S and U configuration points to the far left; as a consequence signals emanating from the SN point no longer fall into the basin of attraction of S, prompting another exocytotic-endocytotic cycle. The limit cycle can have an irregular period by random variation of its associated parameters (SI).

Extended SNARE-SM model predictions. We now test the full model (E-SNARE-SM) with paired whole-cell recordings from both inhibitory and excitatory synapses having differential modes of exocytosis. For inhibition we use recordings from isolated synapses between CCK-positive SCA interneurons in the CA1 region of P18-21 rat hippocampus [16] (see Methods) and we base the model on parameters associated with $GABA_A$-induced currents [16, 35, 36]. For excitation we use data from experiments on calyx-of-Held synapses [4]. The SNARE-SM model parameters are adjusted to generate the appropriate release mode (Table S1) and the MT-model parameters are adopted from [37] as a baseline (SI). Note that asynchronous release is known to be accompanied by irregularity in both, neurotransmitter release times and amplitudes of IPSPs and EPSPs; therefore associated parameter values can vary substantially between release events. The remaining parameters are tuned within a bounded region (Table S2 for inhibitory synapses, and Table S3 for excitatory synapses). Details of the parameter fitting procedures are provided in SI.

The E-SNARE-SM model successfully reproduces the synaptic dynamics of the SCA inhibitory synapse (Fig.4). The delayed unitary inhibitory postsynaptic potential (uIPSP) in Fig.3-a1 is compared with the output of the inhibitory model (Fig.4-b1). A sequence of IPSPs exhibiting short-term synaptic depression and delay in response to multiple presynaptic stimuli (Fig.4a2) matches the output of the model in Fig.4-b2. Responses to a sequence of IPSPs featuring short-term synaptic facilitation and delay, shown in Fig.4-a3, is compared with the response of the model in Fig.4-b3. The model reproduces the onset of the delays and the temporal profile of the IPSPs data. Care was taken with fitting delayed release since the model is sensitive to initial conditions. Completion of an exocytotic-endocytotic cycle brings the system to a different configuration. This implies that parameters of the previous exocytotic-endocytotic cycle will give rise to a different delayed response upon a new stimulus. This can be understood as representing the changes in the exocytotic-endocytotic signalling that occur between subsequent release cycles. Parameters associated with $GABA_A$-induced currents also undergo changes, albeit minor, since endocannabinoids increase the input resistance of the cell, docking time of neurotransmitters and affinity.

The parameters of the MT-model also depend on the mode of release. Continuity conditions are enforced to ensure that different epochs of data fit with different modes of release (shaded magenta and cyan rectangles in Fig.4-a2, -b2, -a3, -b3). Future developments will include the conditions ensured by the way-in-way-out function for an automatic parameter fitting. However, in the limit of complete depletion of neurotransmitters, fitting any continuous mesoscopic model to electrophysiological data becomes increasingly difficult, because noise dominates and expressing microscopic dynamics becomes fundamental (see averaging effect in Fig. S10). In this limit, other theoretical studies reveal that discrete, stochastic or agent-based models best describe microscopic activity [38].

Comparisons between excitatory postsynaptic currents (EPSC) at the calyx-of-Held synapse and the postsynaptic currents of the E-SNARE-SM model are made in Fig.5. Specifically, Fig.5a1 depicts a synchronous activation to a single presynaptic spike, which is matched by the model in Fig.5-b1. Multiple postsynaptic activations elicited by a single input are shown in Fig.5-a2. The first postsynaptic activation is asynchronous and the two subsequent releases are spontaneous. The model is in good agreement over three epochs shown in different colors (Fig.5-b2). Moreover, the model can also reproduce the wild-type data from the calyx of Held. In particular, the strong synaptic depression seen at this synapse during high-frequency stimulation and the kinetics of recovery from synaptic depression can both be captured. Indeed our model builds upon the MT framework which has been shown to account for these phenomena [39].

Discussion

The proposed multiple-timescale SNARE-SM model extends the MT framework for STSP by incorporating all three forms of exocytosis at the same mesoscopic level of description [37]. Moreover, our mathematical model is in good agreement with the biological SNARE-SM model by T. Südhof (compare again Fig.3 and Fig.S1-c with Fig.S1-a). Details of the biochemical pathways involved in exocytosis are semi-phenomenologically expressed and therefore predictions of the model can be compared to SNARE-SM physiology and computational hypotheses can be explored to propose novel experiments. For example, in the model the three distinct forms of release share the same exocytotic machinery, where the modes of exocytosis are controlled by parameters. This suggests that in every exocytosis-endocytosis cycle, the release mode may switch due to slowly-varying physiological variables that have not yet been identified. However, it is important to be cautious since there may be different vesicle pools or pathways (e.g. different calcium sensors) [4].

The timescale parameter ε modulates the activity-induced transcritical canard, which mechanistically explains the ratio between synchronous and asynchronous release. The way-in-way-out function quantifies how the exocytotic-endocytotic signalling pathway fine tunes the timing of neurotransmitter release, which can be seen as a homeostatic mechanism for efficient neuronal communication. This is consistent with molecular studies, showing that within the canonical fusion machinery, synaptotagmin (Syt1) and complexin are functionally interdependent and are potentially the key players in regulating all modes of release [19]. Specifically, Syt1 mediates calcium triggered release and controls the rate of spontaneous release (i.e. speed and precision of release by associations with SNARE complexes). Complexin is a cofactor for Syt1 that functions both as a clamp and as activator of calcium triggered fusion [19].

Further upstream, other proteins could signal (via yet unknown interactions) this homeostatic system. For example, studies show that Syn I(II), known to coat synaptic vesicles and to have post-docking role, regulate synchronous and asynchronous release [15]. In particular, Syn II interacts directly with P/Q-type and indirectly with N-type Ca^{2+} channels to increase asynchronous release. Additionally, Syn I(II) seem to constitute a push-pull mechanism regulating the ratio between synchronous and asynchronous release [15], thus suggesting that they share exocytotic mechanisms. Deeper insight into this mechanism could result from further molecular studies

investigating the existence of a signalling pathway between CB1 receptor, Syn I(II), RIMs and RIM-BS proteins, since CB1 also appears to interact with N-type and P/Q-type Ca^{2+} channels [40, 41]. Nevertheless, multiple exocytotic mechanisms should not be ruled out and augmenting the proposed model to allow switching between them is a focus for future research.

The proposed model could also be mapped onto the dual-calcium-sensor model [4]. Another reported mechanism that should be considered is the VAMP4-enriched vesicle pool, which is formed after intense stimulation and enable asynchronous release [11]. Surprisingly, the authors show that VAMP4-driven SNARE complexes do not readily interact with synaptotagmin and complexin, which challenges the widely-held view that synchronous release requires interaction of SNARE complexes (e.g. VAMP4-SNAP-25 and syntaxin-1) with synaptotagmin-1 and complexins. This issue could be resolved by seeking an alternative way to elicit VAMP4-mediated release (identifying a different signalling pathway). In view of the present model, it would be relevant to test for VAMP4 in synapses expressing CCK. Despite these observations, the SNARE-SM model can explain these results without assuming the existence of a second, VAMP4-enriched pool of vesicles (Fig.S8). Another refinement may emerge from a recent study showing that 2-AG/anandamide directly modulates $GABA_A$ postsynaptic receptors, therefore affecting neurotransmitter docking times and possibly contributing to asynchronicity [42]. Other forms of synaptic plasticity, such as spike-timing-dependent plasticity (STDP) mediated by differential exocytosis, could also be explored with the proposed model (Fig.S9).

Finally, the SNARE-SM model will facilitate large-scale network simulations and consequently explain the functional role of differential exocytosis and synaptic plasticity on network states and how these relate to memory, cognition and pathological brain states (e.g. epilepsy) [43]. At a micro-scale, the proposed theoretical approach could provide new insights into the function of other protein-protein interactions. For example, activity-induced transcritical canards, can explain recent experiments that identify proteins mediating the asynchronous activation of sodium and potassium channels [44].

Materials and Methods

Inhibitory synapses:

Experimental preparations and observations: The data is sampled from paired whole-cell recordings obtained from unitary synapses between CCK-positive SCA interneurons in the CA1 region of P18-21 rat hippocampus [45] (Fig.S10). These cells possess a modulatory feedback mechanism that allows the post-synaptic cell to control the level of pre-synaptic $GABA_A$ release via the endocannabinoid (eCB) system, which is composed of cannabinoid receptors, ligands and the relevant enzymes [45]. Specifically, endocannabinoid, 2-arachidonoyglycerol (2-AG) or anandamide is synthesised and released on demand, involving depolarisation of the postsynaptic membrane via the activation of voltage-dependent L-type calcium channels [46]. Once synthesised it diffuses across the synaptic cleft to modulate the activation of cannabinoid type 1 (CB1) receptors located in the pre-synaptic cell. Subsequently, CB1 receptors inactivate N-type (and possibly P/Q type) calcium channels (therefore reducing Ca^{2+} concentration) leading to a reduction of $GABA_A$ release [45]. Experimentally, the level of CB1 receptor activation and deactivation was controlled by bath application of endogenous agonist, anandamide and antagonist, AM-251. The endogenous agonist effects could be mimicked by depolarisation-induced suppression of inhibition (DSI) protocols, which involved depolarisation of the postsynaptic membrane [45]. These modulatory synaptic effects have a direct impact on the timing of synaptic inhibition, specifically, asynchronous release and STSP (Fig.S10). Details of the experimental preparation is explained.

Slice preparation: Male Wistar rats (P18 - P23, Harlan, UK) were anaesthetised with sodium pentobarbitone (60mg/kg Euthatal, Merial, UK) via intraperitoneal injection and perfused transcardially with ice-cold modified artificial cerebral spinal fluid (ACSF), containing (in mM): 15 D-glucose, 248 sucrose, 2.5 CaCl2, 3.3 KCl, 1.2MgCl2, 25.5 NaHCO3 and 1.4 NaH2PO4. Following decapitation, the brain was removed and 300μm thick coronal slices of cerebral cortex were cut. These procedures were performed under UK Home office guidelines by authorised Home office licence holders. The severity of the procedures was classed as moderate. The total number of rats used for this study was 61. Slices were incubated for 1 hour prior to recording, for which they were placed in a submerged chamber perfused with ACSF at a rate of 1-2 mLmin-1. ACSF contained (in mM): 20 D-glucose, 2 CaCl2, 2.5 KCl, 1 MgCl2, 121 NaCl, 26 NaHCO3, and 1.25 NaH2PO4 (equilibrated with 95% O2 and 5% CO2). All substances used to make ACSF solutions were obtained from VWR, UK (See [45]).

Electrophysiological recordings: Electrodes with resistances of 8-11MΩ were pulled from borosilicate glass and filled with an intracellular solution containing (in mM): 144 K-gluconate, 0.2 EGTA, 10 HEPES, 3 MgCl2 0.2 Na2-ATP, 0.2 Na2-GTP, and 0.02% w/v biocytin (pH 7.2 - 7.4, 300mOsm). Slices were viewed using video microscopy under near-differential interference contrast (DIC) illumination to enable cells to be chosen based upon the shape of their soma and dendritic projections. Neurons were further identified by their firing properties following a series of 500ms depolarizing current steps from +0.05nA to +0.15nA. Dual whole cell recordings were performed in current clamp at room temperature in CA1 stratum radiatum and lacunosum moleculare border. Presynaptic action potentials were generated by a depolarizing current injection of varying length (5-10ms) to enable Inhibitory Post Synaptic Potentials (IPSPs) to be observed in response to single, double or trains of action potentials. Connections were tested in both directions for all pairs. Data were acquired with SEC 05L/H amplifiers (npi electronics, GmbH). Recordings were filtered at 2KHz, digitized at 5KHz using a CED 1401 interface and stored on a hard disk drive. Input resistances were continually monitored by injecting a small hyperpolarizing current injection at duration of 20ms at the start of each frame.

Pharmacology: The endogenous CB receptor agonist, anandamide (in water soluble emulsion) (14μM) was used. AM-251 (1-(2,4-dichlorophenyl)-5-(4-iodophenyl)-4-methyl-N-(1-piperidyl)pyrazole-3-carboxamid, Tocris, UK), a selective CB1 receptor inverse agonist was dissolved in DMSO, stored as stock at -20C and bath applied at 10μM. AM251 is structurally very close to SR141716A, a cannabinoid receptor antagonist, but exhibits a higher binding affinity for the CB1 receptor with a Ki value of 7.5nM compound to SR141716A, which has a Ki value of 11.5nM.

Electrophysiological data analysis: Using Signal (CED), the electrophysiological characteristics of the recorded cells were measured from their voltage responses to 500ms current pulses between -0.2 and +0.1nA in amplitude. Postsynaptic events were either accepted for analysis or rejected. Individual sweeps were observed and either accepted, edited, or rejected according to the trigger points that would trigger measurements and averaging of the IPSPs during subsequent data analysis. Averaging of IPSPs was triggered from the rising phase of the presynaptic spike. Apparent failures of synaptic transmission were counted manually, IPSP amplitudes in the range of the synaptic noise were taken as failures. Selection and averaging of these apparent failures resulted in no measurable postsynaptic responses. Single sweep IPSP amplitudes were measured from the baseline to the peak of the IPSP and are displayed as $\pm$ SD. IPSP half width and the 10-90% rise time were obtained from averages created from 100-300 sweeps. IPSP latencies were manually measured as the time delay between presynaptic action potential peaks to the onset of the detectable IPSPs. The fluctuations in the IPSP latencies were quantified in non-overlapping time interval sets of 5 ms after each presynaptic action potential. Synchronous release was taken as release of neurotransmitter within [0-5)ms latencies, whereas asynchronous release was taken as the release of neurotransmitter falling within a time window of [5-15)ms latencies [40]. The synchronicity ratio was calculated as the ratio of synchronous release/asynchronous release (from data set of 100-300 sweeps).

Excitatory synapses: Recordings were performed in the lab of Prof. Thomas Südhof at Stanford University. In particular, data in Fig.4-a1 and -a2 were extracted from Fig. 2a, **Syt2** knockout, of [10].

Softwares: Electrophysiological data were acquired and analysed off line using Signal from Cambridge Electronic Design, UK (CED). For model simulations, we used the software package XPPAUT [47]. The parameter fitting of the model from data was carried out with MATLAB.

Acknowledgments

ABA thanks the Medical Research Council (UK) New Investigators Award for funding the experiments. JMC is funded by Ikerbasque: The Basque Foundation for Science. ABA thanks the Medical Research Council (UK) New Investigators Award for funding the experiments. TJS is supported by the Howard Hughes Medical Institute, the National Institutes of Health and the Office of Naval Research. We are grateful

to Dr. Thomas Südhof (Stanford University) for providing voltage-clamp recordings of the calyx-of-Held synapses [4].

1. Pang ZP, Südhof TC (2010) Cell biology of ca^{2+}-triggered exocytosis. Curr Opin Cell Biol 22:496–505.
2. Smith SM, et al. (2012) Calcium regulation of spontaneous and asynchronous neurotransmitter release. Cell Calcium 52:226–233.
3. Sara Y, Virmani T, Deák F, Liu X, Kavalali ET (2005) An isolated pool of vesicles recycles at rest and drives spontaneous neurotransmission. Neuron 45:563–573.
4. Sun J., Pang Z. P., Qin D., Fahim A. T., Adachi R., Südhof T.C. (2007) A dual-Ca^{2+}-sensor model for neurotransmitter release in a central synapse. Nature 450:676–682.
5. Verhage M, et al. (2000) Synaptic assembly of the brain in the absence of neurotransmitter secretion. Science 287:86469.
6. Schoch S, et al. (2001) SNARE function analyzed in synaptobrevin/VAMP knockout mice. Science 294:111722.
7. Bronk P, et al. (2007) Differential effects of SNAP-25 deletion on Ca2^{+}-dependent and Ca2^{+}-independent neurotransmission. J. Neurophysiol. 98:794806.
8. Zhou P, et al. (2013). Syntaxin-1N-peptide and Habc-domain perform distinct essential functions in synaptic vesicle fusion. EMBO J. 32:15971.
9. Broadie K, et al. (1995) Syntaxin and synaptobrevin function downstream of vesicle docking in Drosophila. Neuron 15:66373
10. Vilinsky I, et al. (2002) A Drosophila SNAP-25 null mutant reveals context-dependent redundancy with SNAP-24 in neurotransmission. Genetics 162:25971
11. Raingo J, et al. (2012) Vamp4 directs synaptic vesicles to a pool that selectively maintains asynchronous neurotransmission. Nat Neurosci 15:738–745.
12. Maximov A, et al. (2008) Genetic analysis of synaptotagmin-7 function in synaptic vesicle exocytosis. Proc. Natl. Acad. Sci. USA 105:398691.
13. Pang ZP, et al. (2011) Doc2 supports spontaneous synaptic transmission by a ca^{2+}-independent mechanism. Neuron 70:244–251.
14. Calakos N, et al. (2004) Multiple roles for the active zone protein RIM1α in late stages of neurotransmitter release. Neuron 42:88996.
15. Medrihan L, et al. (2013) Synapsin II desynchronizes neutrotransmitter release at inhibitory synapses by interacting with presynaptic calcium channels. Nat Commun 4:1–13.
16. Ali AB (2007) Presynaptic inhibition of gaba$_\alpha$ receptor-mediated unitary ipsps by cannabinoid receptors at synapses between cck-positive interneurons in rat hippocampus. J Neurophysiol 98:861–869.
17. Kaeser, P. S., and Regehr W. G., (2014) Molecular mechanisms for synchronous, asynchronous, and spontaneous neurotransmitter release. Annual review of physiology 76: 333-363.
18. Lipstein N, et al. (2013) Dynamic control of synaptic vesicle replenishment and short-term plasticity by ca^{2+}-calmodulin-munc13-1 signaling. Neuron 79:82–96.
19. Südhof T. C. (2013) A molecular machine for neurotransmitter release: synaptogamin and beyond. Nature Medicine 19:1227–1231.
20. Krupa M, Szmolyan P (2001) Extending slow manifolds near transcritical and pitchfork singularities. Nonlinearity 14:1473–1491.
21. Desroches M, Krupa M, Rodrigues S (2012) Inflection, canards and excitability threshold in neuronal models. J Math Biol 67:989–1017.
22. Lobry C (1991) Dynamic Bifurcations, E. Benoît, ed. vol. 1493 of Lecture Notes in Math, pp. 1–13, Springer.
23. Benoît E, et al. (1981) Chasse au canard. Coll Math 32: 37–119.
24. Volman V, Gerkin RC, Lau PM, Ben-Jacob E, Bi GQ (2007) Calcium and synaptic dynamics underlying reverberatory activity in neuronal networks. Phys Biol 4:91.
25. Nadkarni S, Bartol TM, Sejnowski TJ, Levine H (2010) modeling vesicular release at hippocampal synapses. PLoS Comput Biol 6(11):1–17.
26. Volman V, Levine H, Sejnowski TJ (2010) Shunting inhibition controls the gain modulation mediated by asynchronous neurotransmitter release in early development. PLoS Comput Biol 6:e1000973.
27. Volman V, Gerkin RC (2011) Synaptic scaling stabilizes persistent activity driven by asynchronous neurotransmitter release. Neural Comput 23:927–957.
28. Nadkarni S, Bartol TM, Stevens CF, Sejnowski TJ, Levine H (2012) Short-term plasticity constrains spatial organization of a hippocampal presynaptic terminal. Proc Natl Acad Sci USA 109:14657–14662.
29. Markram H, Tsodyks M (1996) Redistribution of synaptic efficacy between pyramidal neurons. Nature 382: 807–810.
30. Tsodyks M, Markram H (1997) The neural code between neocortical pyramidal neurons depends on neurotransmitter release probability. Proc Natl Acad Sci USA 94: 719–723.
31. Wang Y, et al. (2006) Heterogeneity in the pyramidal network of the medial prefrontal cortex. Nat Neurosci 9: 534–542.
32. Raghavachari S, Lisman JE (2004) Properties of quantal transmission at ca1 synapses. J Neurophysiol 92:2456–2467.
33. Kasai H, et al. (2012) Distinct initial snare configurations underlying the diversity of exocytosis. Physiol. Rev 92(4):1915-1964.
34. Danglot L, Galli T (2007) What is the function of neuronal ap-3? Biol Cell 99:349–361.
35. del Rio CAC, Lawrence JJ, Erdelyi F, Szabo G, McBain CJ (2011) Cholinergic modulation amplified the intrinsic oscillatory properties of ca1 hippocampal cholecystokinin-positive-positive interneurons. J Physiol 589:609–627.
36. Tricoire L, et al. (2011) A blueprint for the spatiotemporal origins of mouse hippocampal interneuron diversity. J Neurosci 31(30):10948–10970.
37. Markram H, Wang Y, Tsodyks M (1998) Differential signalling via the same axon of neocortical pyramidal neurons. Proc Natl Acad Sci USA 95:5323–5328.
38. Campillo F, Lobry C (2012) Effect of population size in a predator–prey model. Ecol Modell 246:1–10.
39. Hermann J, Grothe B, Klug A (2009) Modeling short-term synaptic plasticity at the calyx of held using in vivo-like stimulation patterns. Journal of neurophysiology 101(1): 20–30.
40. Twitchell W, Brown S, Mackie K (1997) Cannabinoids inhibit n-and p/q-type calcium channels in cultured rat hippocampal neurons. J Neurophysiol 78:43–50.
41. Ali AB (2011) Cb1 modulation of temporally distinct synaptic facilitation among local circuit interneurons mediated by n-type calcium channels in ca1. J Neurophysiol 105:1051–1062.
42. Sigela E, et al. (2011) The major central endocannabinoid directly acts at gaba$_\alpha$ receptors. Proc Natl Acad Sci USA 108(44):18150–18155.
43. Cortes JM, et al. (2013) Short-term synaptic plasticity in the deterministic Tsodyks-Markram model leads to unpredictable network dynamics. Proc Natl Acad Sci USA 110(41):16610–615.
44. Lacroix JJ, Campos FV, Frezza L, Bezanilla F (2013) Molecular bases for the asynchronous activation of sodium and potassium channels required for nerve impulse generation. Neuron 79:651–657.
45. Ali AB, Todorova M (2010) Asychronous release of GABA via tonic cannabinoid receptor activation at identified interneuron synapses in rat CA1. Eur J Neurosci 31: 1196–1207.
46. Lenz RA, Wagner JJ, Alger BE (1998) N- and L-type calcium channel involvement in depolarization-induced suppression of inhibition in rat hippocampal CA1 cells. J Physiol 512: 61–73.
47. Ermentrout B (2002) Simulating, analyzing, and animating dynamical systems: a guide to XPPAUT for researchers and students. SIAM.

Caption of Fig.1 : The parsimonious SNARE-SM molecular exocytotic machinery, (figure modified from [1]). Synaptic vesicles, docked at the active zone of a pre-synaptic terminal, are primed for release by partial SNARE-complex assembly that is catalyzed by Munc18, Munc13 and RIMs. The second stage involves 'superpriming' due to the regulation of complexins on the assembled SNARE complexes, which gives rise to priming stage II. This forms a substrate for either calcium-triggered release via mediation of a calcium sensor, such as synaptotagmins, or spontaneous release, which then enables fusion-pore opening and neurotransmitter release. Subsequently, N-ethyl-maleimide-sensitive factor (NSF) and soluble NSF attachment proteins (SNAPS) mediate disassembly of the SNARE complex, leading to vesicle recycling.

Caption of Fig.2 : Schematic idealisation of the SNARE-SM model. The circular centre describes the canonical fusion machinery constituted by the SNARE complex and SM proteins, which is ultimately regulated by Complexin and Synaptogamins [19]. This building block is signalled by various proteins and, depending on the proteins involved, the appropriate neurotransmitter release mode is activated (i.e. synchronous, asynchronous and spontaneous). Some of the known proteins associated to each type of release are indicated (see review [17] for a complete description and the latest view on the association between proteins and release modes). The proteins RIMs are shared between synchronous and asynchronous release modes, while TRPV1, Doc2 and Voltage-gated Ca^{2+} channels (VDCC) are shared between asynchronous and spontaneous release modes. The remaining proteins are specific to each release mode, however, inhibiting a protein specific to a given release mode will favour the expression of other modes [17].

Caption of Fig.3 : SNARE-SM model dynamics and asynchronous mechanism. (a) Interactions between protein complexes p_1 and p_2 along the vesicle cycle are given by the parabola and the horizontal line (black). These give rise to special points S, U, TC and SN, which mediate all the functions associated with the exocytotic-endocytotic cycle (red curve): Priming (P), Fusion (F), Endocytosis (E) and Refilling (R). Note that priming stage I initiates after point U, while priming stage II initiates after point TC. Arrows indicate dynamic trajectories in the phase plane. (b1) Time course of presynaptic voltage and (b2) p_2 activity following a stimulus. (b3) Schematic diagram of an energy landscape where stimulus spikes are required to activate p_1 and p_2, represented as a particle that initiates movement only if sufficient energy is provided to traverse the energy barrier (U).

Caption of Fig.4 : Model comparison with inhibitory synapse. (a1) Delayed IPSP ($\sim$ 5.6 ms) of CKK-positive SCA interneuron to unitary input spike at time t_{sp} (dashed-red line). (b1) Response of the model to the same input as a1. (a2) Depressed and delayed IPSP data resulting from spikes occurring at times t_{sp_i}, $i = \{1 \dots 5\}$ (red-dashed lines). First epoch (shaded magenta rectangle) is triggered by the first three spikes causing synchronous mode (release within 5 ms); second epoch (shaded cyan rectangle) is initiated by two subsequent spikes that lead to asynchronous mode (more than 5 ms delayed release). Inset: expansion of the region corresponding to the five release events; vertical red-dashed lines mark spike times, vertical blue lines mark IPSP response times. The distance between them measures the delay: $\sim$ (2.0, 2.6, 2.5, 9.2, 15.0) ms. (b2) Response of the model to the same input as a2. (a3) Facilitated and delayed IPSP data. First epoch (shaded magenta rectangle), induced by the first three spikes, leads to synchronous release with delayed response times of $\sim$ (4.2, 3.6, 4.1) ms. The second epoch (shaded cyan rectangle), evoked by two subsequent spikes, with marginal delayed release times ($\sim$ (5.0, 5.1)ms). (b3) Response of the model to the same input as a3.

Caption of Fig.5 : Model comparison with excitatory synapse. (a1) Synchronous EPSC ($\sim$ 1.6 ms) of the calyx-of-Held synapse to unitary input spike at time t_{sp} (dashed-red line). The blue dashed line show the time instant of activation. Data was extracted from Fig. 2a, *Syt2* knockout, of [4]. (b1) Response of the model to the same input as a1. (a2) A unitary input spike at time t_{sp} (dashed-red line) first causes a delayed EPSC (at $\sim$ 4 ms) and further two spontaneous activations $\sim$ (27.3, 41.3) ms. Data was extracted from Fig. 2a, *Syt2* knockout, of [4]. (b2) Response of the model to the same input as a2. Here the different epochs of the data reflect the transitions from delayed (shaded magenta rectangle) to spontaneous activation (shaded cyan and shaded light orange rectangles). The model replicates this by varying the parameters of the SNARE-SM model that dictate the transition from delayed to spontaneous regime (Table S1).

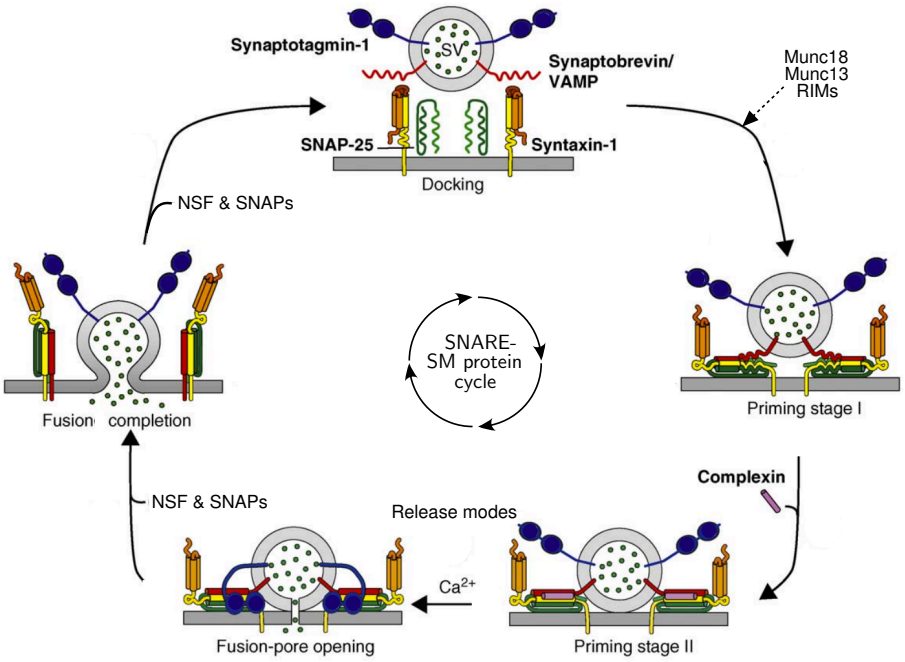
Synaptotagmin-1
SV
Synaptobrevin/
VAMP
Munc18
Munc13
RIMs
SNAP-25
Syntaxin-1
Docking
NSF & SNAPs
SNARE-
SM protein
cycle
Priming stage I
Fusion completion
Complexin
NSF & SNAPs
Release modes
Ca2+
Fusion-pore opening
Priming stage II

Fig. 1.

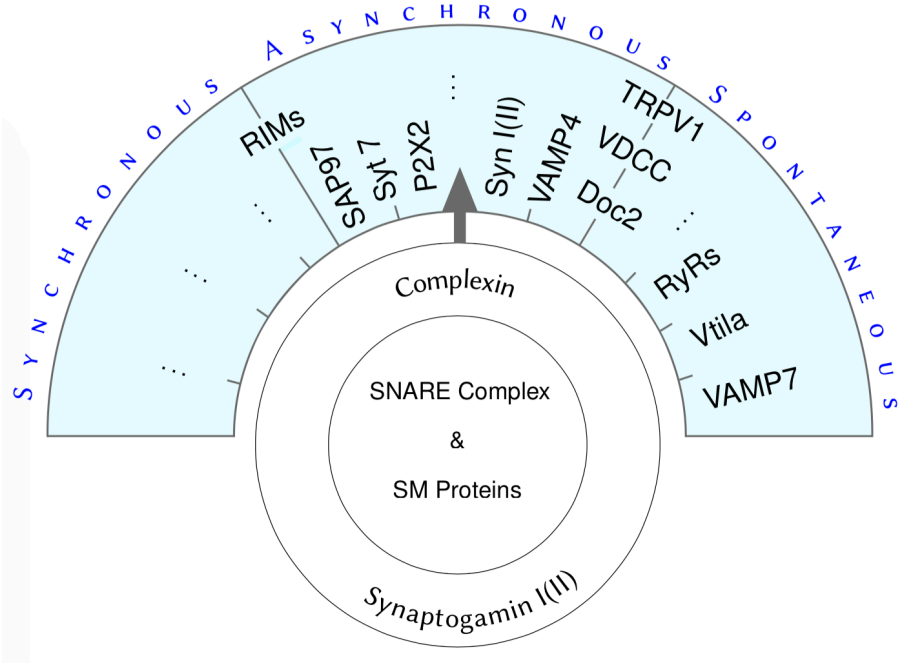
SYNCHRONOUS
ASYNCHRONOUS
SPONTANEOUS
RIMs
SAP97
Syt 7
P2X2
Syn I(II)
VAMP4
Doc2
VDCC
TRPV1
RyRs
Vtila
VAMP7
Complexin
SNARE Complex
&
SM Proteins
Synaptogamin I(II)

Fig. 2.

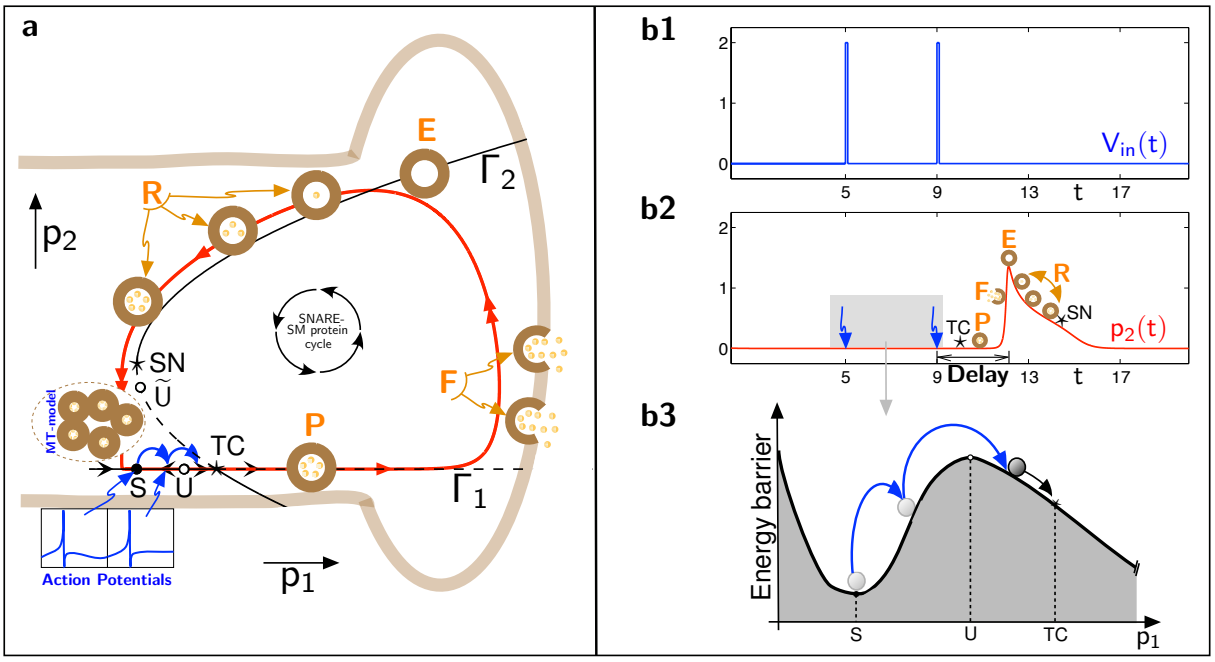
a
E
Γ2
R
p2
SNARE-
SM protein
cycle
SN
Ũ
MT-model
F
TC
P
S
U
Γ1
Action Potentials
p1
b1
2
1
0
Vin(t)
5
9
13
t
17
b2
E
F
R
SN
TC
P
p2(t)
Delay
b3
Energy barrier
S
U
TC
p1

Fig. 3.

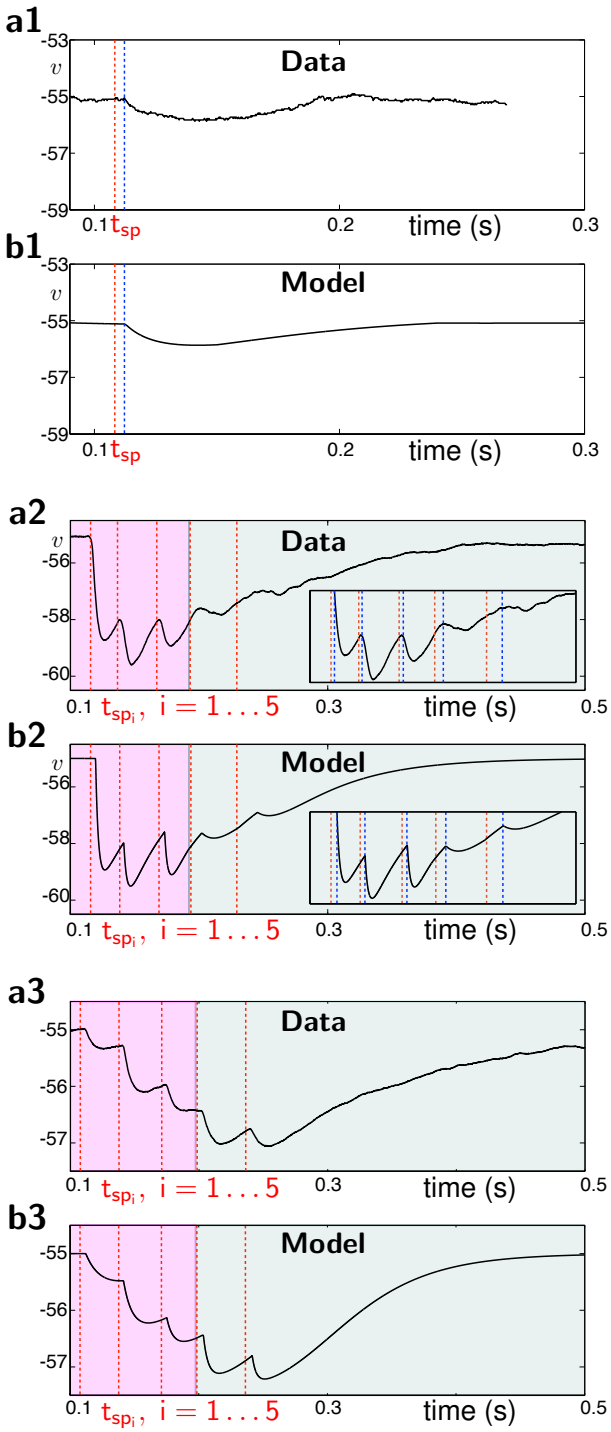
a1
Data
b1
Model
a2
Data
b2
Model
a3
Data
b3
Model
v
time (s)
t_{sp}
t_{sp_i}, i = 1 . . . 5

Fig. 4.

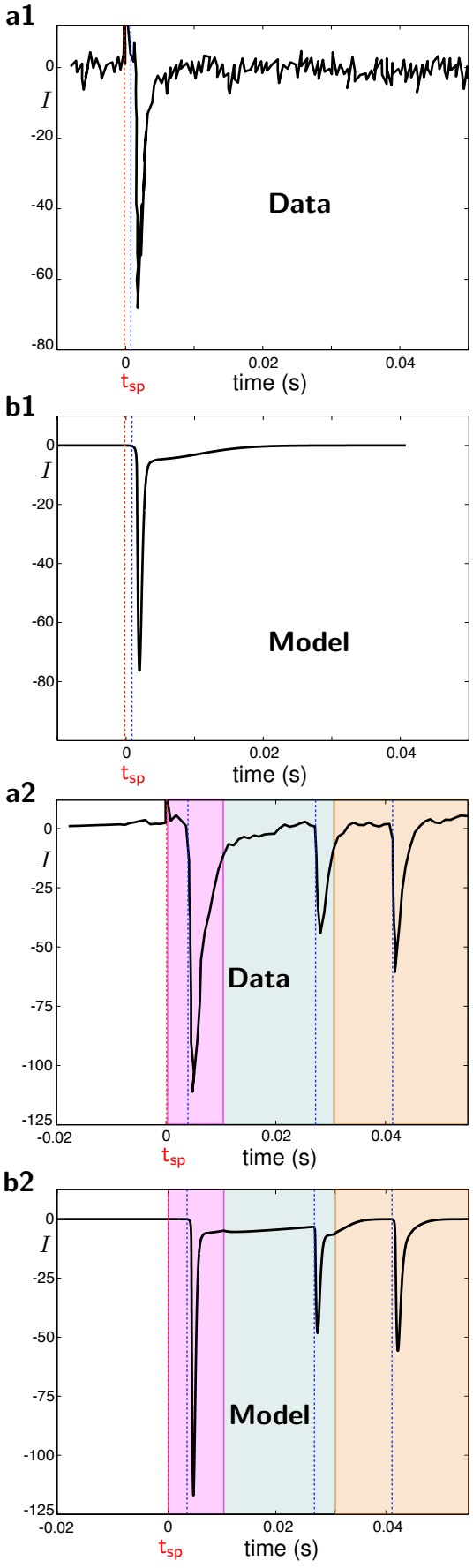
a1
0
I
-20
-40
-60
-80
Data
0
0.02
0.04
t_sp
time (s)
b1
0
I
-20
-40
-60
-80
Model
0
0.02
0.04
t_sp
time (s)
a2
0
I
-25
-50
-75
-100
-125
Data
-0.02
0
0.02
0.04
t_sp
time (s)
b2
0
I
-25
-50
-75
-100
-125
Model
-0.02
0
0.02
0.04
t_sp
time (s)

Fig. 5.